SAND2013-10371C

Development of two-beam femtosecond/picosecond one-dimensional rotational coherent anti-Stokes Raman spectroscopy: time-resolved probing of flame wall interactions

Alexis Bohlin[1], Markus Mann[2], Brian D. Patterson[1], Andreas Dreizler[2], and Christopher J. Kliewer[1*]

[1]Combustion Research Facility, Sandia National Laboratories, Livermore, CA 94551, USA

[2]FG Reaktive Strömungen und Messtechnik, Center of Smart Interfaces, 64287 Darmstadt, Germany

Christopher J. Kliewer* (Corresponding Author*), cjkliew@sandia.gov, (tel) 00 1-925-294-4973 (fax) 00 1-925-294-2276

Name of Colloquium: Diagnostics

Short Running Title: Two-beam fs/ps 1D rotational CARS

Total Length of Paper Using Method 1:

Total Word Equivalent = **5799**

Main Body Text + Figure Captions = 3520

References = 576

Figures = 463+476+169+181+414

Equations = 0

Color Reproduction: Agree to pay color reproduction charges

Submitted for presentation at the

35th International Symposium on Combustion

San Francisco, CA August 3-8 2014

Abstract

Hybrid femtosecond / picosecond rotational coherent anti-Stokes Raman spectroscopy (CARS) is developed utilizing a two-beam phase-matching approach for one-dimensional (1D) measurements demonstrated in an impinging jet burner to probe time-resolved head on quenching (HOQ) of a methane/air premixed flame at Φ=1.0 and Reynolds number = 5000. Single-laser-shot 1D temperature profiles are obtained over a distance of 4 mm by fitting the pure-rotational N_2 CARS spectra to a spectral library calculated from a time-domain CARS code. An imaging resolution of ~61 μm is obtained in the 1D-CARS measurements. The acquisition of single-shot 1D-CARS measurements, as opposed to traditional point-wise CARS techniques, enables new spatially correlated conditional statistics to be determined, such as the position, magnitude, and fluctuations of the instantaneous temperature gradient. The temperature gradient increases as the flame approaches the metal surface, and decreases during quenching. The standard deviation of the temperature gradient follows the same trend, increasing as the flame front approaches the surface, and decreasing after quenching.

Keywords: Time-resolved spectroscopy; CARS; coherent imaging; flame-wall interactions, combustion diagnostics

1. Introduction

Coherent anti-Stokes Raman spectroscopy (CARS) has been developed over the past few decades to become authoritative in terms of the accuracy and precision the technique can achieve in the measurement of gas-phase temperature and major species concentrations in combustion systems. The datasets obtained in such experiments serve as benchmarks for comparison to numerical simulations of combustion, with the aim to provide feedback for improving detailed combustion models. Because of the coherent nature of the CARS signal, the technique is particularly useful in probing highly luminous or scattering environments, such as in sooting flames and combustion near surfaces. Several historical limitations in the CARS technique have recently been addressed and improved: spatial resolution, single-shot precision, sensitivity to collisional environment, and the point-wise dimensionality of the data acquisition. Each improvement is discussed in the following.

In the early days of CARS development, a collinear beam geometry was implemented. Such a scheme is intrinsically phase-matched, and generates very large CARS signal levels; however, the spatial sectioning of the probed location is typically on the order of centimeters, which is not adequate to resolve the spatial scales of interest in combustion studies. The three-beam folded BOXCARS phase matching scheme was then developed

[1] to improve the spatial resolution, enabling a crossed beam geometry with intrinsic spatial sectioning of the probed location. CARS signal is generated only where the three beams cross, and the spatial resolution of experiments implementing this arrangement has typically been on the order of millimeters (mm), although this can be improved by going to steeper crossing angle. The CARS phase matching scheme has been recently revisited, and a counter-propagating CARS arrangement (counter-propagating pump and Stokes beams) was demonstrated [2] reducing the interaction length (spatial resolution along the probe beam-propagation direction) to 155 μm, and yielding high signal levels for 1D imaging applications. Subsequently, a two-beam rotational CARS phase matching scheme was developed [3] which allows for tunability of the spatial resolution down to ~50 μm if desired, set by the crossing angle between the pump/Stokes and probe beams. The CARS signal level decreases quadratically with the probed volume, therefore balancing of the desired spatial resolution and signal level is required.

The implementation of near-transform limited femtosecond pulses for coherence excitation benefits from the multitude of photon pairs which contribute in phase to drive a particular coherent transition. The result is a significant improvement in the shot-to-shot stability of the CARS spectrum with low mode-noise, such as often limits the precision of measurements where broadband dye lasers are used. In the evaluation of temperature from femtosecond vibrational [4] and rotational [5] CARS spectra, this improvement has been demonstrated to yield a single shot standard deviation of less than ~1%, as compared to the 3-4% standard deviation typically reported in nanosecond CARS experiments [6] and picosecond CARS experiments [7, 8].

The accurate interpretation of CARS spectra requires knowledge of the Raman linewidths of the probed transitions which are dependent on the local collisional environment. With nanosecond CARS, it has been shown that properly accounting for the collisional environment by weighting the Raman linewidths for the gas composition can yield a systematic and significant improvement in the accuracy of evaluated temperatures from CARS spectra [9]. One key advantage of time-resolved CARS in this regard is the capability to directly measure the collisional dephasing of coherences by monitoring the signal as a function of probe delay. In this manner, the Raman broadening coefficients for self-broadened N_2 [10, 11], O_2 [12], H_2 [13], and CO_2 [14] as well as intermolecular broadening coefficients for N_2-H_2 [15] and CO_2-N_2 [14] have been recently measured for a variety of temperatures and pressures. For picosecond CARS, as well as femtosecond/picosecond CARS, an accurate

model of the Raman linewidths is required for accurate spectral interpretations, especially at elevated pressure. The total broadening coefficient can be measured *in-situ* during a stable combustion experiment by utilizing a probe-delay scan, and this has been demonstrated in a sooting ethylene diffusion flame [16] with temperature corrections of up to 125K in the evaluation of picosecond CARS spectra when compared to analysis incorporating a standard N_2 self-broadened linewidth model. In cases where the flame is unsteady, a split-probe CARS scheme has been developed for measuring Raman broadening coefficients on the basis of a single-laser-shot [17].

Another limitation of CARS applications to the study of combustion has been that of dimensionality. Gas-phase CARS has almost exclusively been implemented as a point-wise measurement technique, whereas combustion is only fully characterized in three-dimensional space. The most significant difficulty in moving from point-wise to 1D measurements in the past has been the significant decrease in signal level. The first reported attempt for 1D rotational CARS was made by Snow *et al*. [18] using a nanosecond CARS laser system; however, low signal levels permitted measurements only at low temperature and over a distance of 1.8 mm. The high peak intensity of picosecond pulses allows for high CARS signal intensities at relatively low pulse energies for picosecond CARS, motivating a 1D imaging setup. 1D picosecond rotational CARS was demonstrated in our lab [2, 7] by imaging a field of view of 12-20 mm within a single laser shot at temperatures of up to 1500K. Once again, however, overall signal levels were a difficulty in these experiments, and implementation for single-shot measurements at flame temperatures over 2000K was not readily obtainable for a distance of several mm. By combining the extremely high CARS signal levels obtained by impulsive femtosecond excitation of rotational Raman coherences with a high-energy picosecond probing pulse, we have recently demonstrated femtosecond/picosecond 1D rotational CARS in a single laser shot at typical adiabatic flame temperatures [3] over a several mm field of view. In this work, we develop a two-beam femtosecond/picosecond 1D rotational CARS scheme for probing the near-surface region of an impinging jet burner during time-resolved head on quenching studies.

Interaction of turbulent premixed flames with solid walls is of primary interest for spark-ignition IC engines and low-NOx gas turbine combustion. Increasing power densities enlarge surface-to-volume ratios. In turn the impact of walls on fluidic, thermodynamic and thermo-chemical properties of flames is of increasing importance. Compared to unbound turbulent flames, flame-wall interactions (FWI) are much less studied. Of primary interest

are heat losses by conduction that cause flame quenching at the wall [19]. Heat fluxes have been measured by sensors integrated into the wall, see for example [20, 21]. Gas temperatures near walls have been measured by laser-induced fluorescence [22] and by point-wise nanosecond CARS [23, 24]. One-dimensional recording of wall-normal temperature profiles with high spatial resolution to resolve steep gradients associated with the thermal boundary layer would enable the study of instantaneous flame structures near walls. This would greatly guide model development and understanding of interaction of flames with walls.

2. Experimental

HOQ and side-wall quenching are the two canonical configurations for studying flame-wall interactions. In this study the focus is on HOQ. To constitute HOQ a jet impinges perpendicularly at a cooled steel wall. In our realization the jet issues from a contoured nozzle [25]. The nozzle exit diameter is 30 mm. Inside of the nozzle a turbulence generating plate can be installed to intentionally increase turbulent velocity fluctuations and decrease integral length scales. Using a perforated plate with hexagonally arranged holes (4 mm diameter, 5.2 mm spacing, 45% blocking ratio) length scales at the nozzle exit are at the order 4.7 mm as measured by hot wire anemometry [26]. Methane (purity 99.9%) and dried air are perfectly mixed before entering the nozzle assembly. Flow rates of both gas components are controlled by electronic mass flow controllers (MKS) and can be varied in a wide range spanning from laminar to turbulent conditions. The mass flow controllers were calibrated with a flow verifier (MKS type GBROR). The nozzle is surrounded by coflowing nitrogen to minimize mixing with ambient air.

The wall is positioned 32 mm downstream of the nozzle exit. It is slightly curved (R = 300 mm) to allow for optimum optical access near the wall at centerline. The plate extends 60 mm in radial direction whereas the present study is focused only at centerline profiles. From its back the plate is water-cooled (300K) to guarantee stable boundary conditions.

Prior to HOQ a stationary wall-stabilized flame was investigated. Stationary flames in the present context are particularly useful to investigate the performance of the innovative 1D CARS thermometry. Of primary interest are pulse-to-pulse fluctuations that are needed for evaluating precision of temperature measurements near walls. Following the stationary wall-stabilized flames, HOQ was investigated. For this purpose the continuous flow of premixed gases was ignited 2 mm above the nozzle center. For ignition, the fundamental of a q-switched Nd:YAG

laser (Continuum, Surelite) was focused (f = 100 mm) into the gas. Subsequently the flame propagated to the wall. When the flame first sensed the wall, heat conduction lowered its temperature until the flame quenched back from the surface. After the 1D-CARS single-shot measurement was taken, the flame was blown off automatically by another time-synchronized nozzle. The blow-off nozzle would extinguish the flame and a delay of one second was allowed for the burner to return fully to an undisturbed state.

The burner was operated at Reynolds number 5,000 for both lean (Φ=0.8) and stoichiometric (Φ=1.0) laminar conditions. For each stoichiometry, the stationary flame was analyzed with 1,000 single-laser-shot acquisitions. For the HOQ studies, ~30 time delays after the ignition pulse were studied, covering the propagation of the flame to the steel surface, and the subsequent quenching back to the stationary wall-stabilized position.

Two-beam CARS phase-matching in a 1D configuration [3] was employed in these experiments. The pump/Stokes pulse was taken from a femtosecond regenerative amplifier (Wyvern 1000, KM Labs). The pulse duration was 45 femtoseconds, and pulse characteristics were monitored online with a Grenouille (Swamp Optics). The amplifier was operated at 1 kHz repetition rate and with 3 mJ/pulse output. The full 3 mJ output was focused to the experimental probe volume with a cylindrical lens f = 300 mm. The narrowband probe beam was generated by a picosecond regenerative amplifier. The picosecond and femtosecond oscillators were phase locked to the same 100 MHz RF source allowing for precise electronic timing between the femtosecond and picosecond pulses at the experiment with low jitter (< 1 ps). The 1064 nm output of the picosecond Nd:YAG was doubled to 532 nm and focused to the experiment using a f = 300 mm cylindrical lens. The probe laser was operated at 30 mJ/pulse. The beams were focused to ~50 μm at the experiment as measured with a beam profiling camera (WinCam D). In the two-beam CARS arrangement, the signal is generated collinearly with the probe beam and can be fully isolated from the probe radiation using a polarization gate. The probe beam was set to +45˚ while the pump/Stokes remained vertically polarized at 0˚. The resonant and nonresonant signals thus appeared at -27˚ and 18˚ respectively. A polarization analyzer was placed in the signal path transmitting polarization orthogonal to the probe pulse. This results in a near total (>1:10^6) suppression of the probe pulse, 89% suppression of the nonresonant background, and a 44% reduction in resonant signal.

The signal was then directed through an angle-tuned short-wave-pass filter (Semrock) to eliminate any scattered 532 nm light from reaching the detector while still detecting signals down to ~15 cm^{-1}. A 75-mm focal length cylindrical lens was used to focus the signal through the spectrometer slit. A 1-m spectrometer (Spex 1000M) was used with an 1800 groove/mm grating to disperse the rotational CARS signal onto a CCD camera (Andor Newton). The pixel size on the CCD chip was 16 μm, and the measured dispersion was 0.29 cm^{-1}/ pixel. The dispersion was calculated by comparison to a rotational CARS spectrum taken in room air. The vertical dimension was relay imaged from the experimental probe volume to the spectrometer slit with 1:1 imaging. An air force target was placed at the experimental probe volume and illuminated with white light to characterize the quality of the imaging optics, as well as provide a calibration for any magnification of the imaging system. A linespread function of ~61 μm was evaluated for the system. Each single-laser-shot produced a CCD image with 400 spectra, and a binning of 2x2 was used yielding 200 individual spectra per shot. Figure 1a displays the CCD image of the dispersed 1D signal taken during static wall-stabilized operation of the burner at Φ=0.8. Starting from the bottom of the image, room temperature unreacted gases are flowing in this region. At ~5 mm from the surface a drastic change is observed in the image as the Raman lines populate to much higher shift, corresponding to rotational transitions of higher energy, marking higher temperatures caused by the flame front. Near the surface, located at 0 mm in the image, the populated transitions are observed moving back to lower shift, indicating a rapid cooling, which is caused by the heat transfer to the cooled surface and quenching. Two examples of line-spectra representative at high and low temperature, respectively from this image are shown in Fig. 1b.

3. Theoretical Considerations

Each laser shot in the current experiments produced an array of 200 rotational CARS spectra, and 1000 laser shots were recorded for each condition and ignition delay. The dataset amounted to several million individual spectra, of which all needed to be fit to our time-domain rotational CARS model. A non-linear interpolating method based on a spectral library was required, determining the temperature from a least-square error minimization fitting procedure, commonly employed in nanosecond CARS [27]. The contour of the integrated line-intensities from each of the library spectra were normalized and compared to the distribution of the measured

spectrum in the fitting routine. The time-domain rotational CARS code used for generating the spectral library is similar to that presented in earlier works [5, 10, 28]. The probe delay in these experiments was set to 340 ps. This ensured the full suppression of the nonresonant background as well as the balancing of signals from both cold and hot zones of the reacting flow [3]. The nonresonant susceptibility was omitted from the calculation of the CARS response, as it is negligible for such long probe delays in femtosecond/picosecond CARS. For these first experiments, the modified exponential gap law [29] was used for determining the N_2 linewidths used in the calculation, which is based upon N_2 self-broadening linewidths and the parameter set used can be found in [30]. Herman-Wallis factors were employed to address the breakdown of the rigid-rotor approximation [31]. The experimental spectra were corrected for the finite bandwidth of the excitation effeciency profile and any transmission characteristics of the signal detection path by dividing the measured spectra by a spectrum recorded in pure methane.

4. Results and Discussion

Figure 2 displays the results of femtosecond/picosecond 1D rotational CARS measurements of both the static wall-stabilized and HOQ cases in the FWI burner at stoichiometric (Φ=1.0) condition. The mean temperature profiles converged out of 100 single-shots as a function of distance from the wall and ignition delay are presented in Fig. 2a, while the standard deviation for each data point is presented in Fig. 2b. In both panels, the top bar represents the static, wall-stabilized, case. Inspecting Fig. 2, the flame front can be followed progressing towards the surface at increasing time, and then quenching away from the surface at longer times. Time zero is defined as the ignition delay where the maximum temperature reached closest to the surface. Negative times are prior to quenching. Spatially, each bin corresponds to a 35 μm segment sampled along the 1D probed location. The temperature reaches a maximal value of ~2100K, in good agreement with previous Cantera simulations [24]. 100 single-shot 1D temperature evaluations are displayed in Fig. 3 at a time (t = -2.7 ms) when the flame is freely propagating to the wall.

Comparison of the current femtosecond/picosecond 1D-CARS measurements to previous time-averaged nanosecond CARS and numerical simulation data is shown in Fig. 4 for the fuel equivalence ratio Φ=1.0 and static wall-stabilized operating conditions. 100 single-shot 1D-CARS profiles were averaged for the comparison.

Overall quantitative agreement is found between the temperature profiles, although local differences between the profiles can be seen. For instance, at z = 2 mm in Fig. 4 the 1D-CARS evaluated temperature is ~5% below the previous point-wise CARS data. The local variations between profiles might be attributable to different spatial scales of the two techniques, as well as possible beam steering, spatial averaging, or pulse dispersion effects, to be explored more deeply in future work.

One of the key benefits of single-shot 1D probing when compared to point-wise experimental techniques is the ability to obtain statistical information regarding spatially correlated data, which may allow for a deeper comparison to the numerical simulation of dynamical combustion processes such as HOQ. For instance, it is possible to determine the flame front position and temperature gradient within each laser shot, and thus fluctuations in either the flame front position or gradient can be isolated from each other directly from the experimental data, and statistics conditional upon flame front position can be obtained. Figure 5 demonstrates such data from the present experiment. In Fig. 5a, the flame front position as a function of ignition delay time is determined by taking the derivative of the temperature profile with respect to position, $\Delta T/\Delta z$. The position where $\Delta T/\Delta z$ is at maximal absolute value was identified as the flame front position for negative times. After quenching, the flame extinguishes at the radial center region and $\Delta T/\Delta z$ is a measure of the remaining temperature gradient. The magnitude of $\Delta T/\Delta z$ at this location is the temperature gradient, and the temperature gradient as a function of ignition delay time is displayed in Fig. 5c. The units of $\Delta T/\Delta z$ are given in Kelvin / bin and the conversion factor for spatial scales is 35.2 μm/bin given the measured magnification of our imaging optics. In Fig. 5b and 5d, the standard deviation in flame front position and mean maximum temperature gradient, respectively, are shown as a function of ignition delay time based upon the analysis of 100 individual single-laser-shots.

The slope of the line in Fig. 5a at negative Δt yields the flame velocity. Of course, an alternative method to the maximal temperature gradient technique for visualization of flame front position is to plot the progression of an isotherm. The fluctuations in the position of maximum temperature gradient are observed to grow substantially immediately after the quenching process as seen in the difference in intensity at negative and positive Δt in Fig. 5b. After ignition, as the flame freely propagates towards the surface, the flame front temperature gradient remains relatively constant, but becomes steeper as it approaches the surface as can be seen between Δt=-1.5 ms

and Δt=0 in Fig. 5c. Following the quenching process, the temperature gradient near the surface becomes lower than that of the freely propagating flame. At this stage the flame extinguished and the temperature profile is determined by diffusion processes. Finally, the standard deviation in the temperature gradient is observed to increase from negative Δt to Δt=0, and then decrease following quenching.

5. Summary

We have demonstrated a new capability implementing two-beam femtosecond/picosecond 1D rotational CARS to probe quenching processes. Time-resolved measurements of HOQ in a methane/air premixed flame at Reynolds number 5,000 impinging on a cooled steel surface were performed. Single-laser-shot 1D temperature profiles were obtained as a function of ignition delay, and compared to previous time-averaged nanosecond CARS point-wise measurements with quantitative agreement. The extraction of spatially correlated (1D) conditional statistics, such as fluctuations in the instantaneous flame front temperature gradient as a function of ignition delay, was demonstrated.

Acknowledgements

Funding for CJK and AB provided by the U.S. Department of Energy, Office of Basic Energy Sciences, Division of Chemical Sciences. Sandia is a multiprogram laboratory operated by Sandia Corporation, a Lockheed Martin Company, for the U.S. Department of Energy's National Nuclear Security Administration under contract DE-AC04-94AL85000. AD and MM gratefully acknowledge the financial support of the DFG (Deutsche Forschungsgemeinschaft), EXC 259 (Center of Smart Interfaces) and GRK 1344.

References

1. A. C. Eckbreth, Appl. Phys. Lett. 32 (7) (1978) 421-423 10.1063/1.90070.
2. C. J. Kliewer, Optics Letters 37 (2) (2012) 229-231
3. A. Bohlin; B. D. Patterson; C. J. Kliewer, J. Chem. Phys. 138 (8) (2013) 081102 10.1063/1.4793556.
4. D. R. Richardson; R. P. Lucht; W. D. Kulatilaka; S. Roy; J. R. Gord, Appl. Phys. B-Lasers Opt. 104 (3) (2011) 699-714 10.1007/s00340-011-4489-0.
5. S. P. Kearney; D. J. Scoglietti; C. J. Kliewer, Opt. Express 21 (10) (2013) 12327-12339
6. T. Seeger; A. Leipertz, Applied Optics 35 (15) (1996) 2665-2671 10.1364/ao.35.002665.

7. C. J. Kliewer; Y. Gao; T. Seeger; B. D. Patterson; R. L. Farrow; T. B. Settersten, Applied Optics 50 (12) (2011) 1770-1778
8. H. U. Stauffer; W. D. Kulatilaka; P. S. Hsu; J. R. Gord; S. Roy, Applied Optics 50 (4) (2011) A38-A48 10.1364/ao.50.000a38.
9. A. Bohlin; P. E. Bengtsson, Proceedings of the Combustion Institute 33 (2011) 823-830 10.1016/j.proci.2010.05.023.
10. J. D. Miller; S. Roy; M. N. Slipchenko; J. R. Gord; T. R. Meyer, Opt. Express 19 (16) (2011) 15627-15640
11. C. J. Kliewer; A. Bohlin; E. Nordstrom; B. D. Patterson; P. E. Bengtsson; T. B. Settersten, Appl. Phys. B-Lasers Opt. 108 (2) (2012) 419-426 10.1007/s00340-012-5037-2.
12. J. D. Miller; S. Roy; J. R. Gord; T. R. Meyer, J. Chem. Phys. 135 (20) (2011) 10.1063/1.3665932.
13. W. D. Kulatilaka; P. S. Hsu; H. U. Stauffer; J. R. Gord; S. Roy, Appl. Phys. Lett. 97 (8) (2010) 10.1063/1.3483871.
14. S. Roy; P. S. Hsu; N. Jiang; J. R. Gord; W. D. Kulatilaka; H. U. Stauffer; J. R. Gord, The Journal of Chemical Physics 138 (2) (2013) 024201 10.1063/1.4774093.
15. A. Bohlin; E. Nordstrom; B. D. Patterson; P.-E. Bengtsson; C. J. Kliewer, J. Chem. Phys. 137 (7) (2012) 074302
16. Y. Gao; A. Bohlin; T. Seeger; P. E. Bengtsson; C. J. Kliewer, Proceedings of the Combustion Institute 34 (2013) 3637-3644 10.1016/j.proci.2012.05.010.
17. B. D. Patterson; Y. Gao; T. Seeger; C. J. Kliewer, Optics Letters 38 (22) (2013) 4566-4569 10.1364/ol.38.004566.
18. J. B. Snow; J. B. Zheng; R. K. Chang, Optics Letters 8 (12) (1983) 599-601 10.1364/ol.8.000599.
19. T. J. Poinsot; D. C. Haworth; G. Bruneaux, Combust. Flame 95 (1-2) (1993) 118-132 10.1016/0010-2180(93)90056-9.
20. W. M. Huang; S. R. Vosen; R. Greif, Symposium (International) on Combustion 21 (1) (1988) 1853-1860 http://dx.doi.org/10.1016/S0082-0784(88)80420-X.
21. M. Salem; S. Staude; U. Bergmann; B. Atakan, Exp. Fluids 49 (4) (2010) 797-807 10.1007/s00348-010-0910-4.
22. T. Fuyuto; H. Kronemayer; B. Lewerich; J. Brubach; T. Fujikawa; K. Akihama; T. Dreier; C. Schulz, Exp. Fluids 49 (4) (2010) 783-795 10.1007/s00348-010-0917-x.
23. R. P. Lucht; D. Dunn-Rankin; R. Walter; T. Dreier; S. C. Bopp, SAE Technical Paper 910722 (1991) 10.4271/910722.
24. A. Singh; M. Mann; T. Kissel; J. Brubach; A. Dreizler, Flow Turbul. Combust. 90 (4) (2013) 723-739 10.1007/s10494-011-9384-6.
25. D. Geyer; A. Kempf; A. Dreizler; J. Janicka, Combust. Flame 143 (4) (2005) 524-548 10.1016/j.combustflame.2005.08.032.
26. D. Geyer. 1D-Raman/Rayleigh experiments in a turbulent opposed jet. Dissertation, TU Darmstadt, Germany, 2005.
27. A. Bohlin; E. Nordström; H. Carlsson; X.-S. Bai; P.-E. Bengtsson, Proceedings of the Combustion Institute 34 (2) (2013) 3629-3636 http://dx.doi.org/10.1016/j.proci.2012.05.016.
28. S. Roy; W. D. Kulatilaka; D. R. Richardson; R. P. Lucht; J. R. Gord, Optics Letters 34 (24) (2009) 3857-3859
29. M. L. Koszykowski; L. A. Rahn; R. E. Palmer; M. E. Coltrin, J. Phys. Chem. 91 (1) (1987) 41-46 10.1021/j100285a012.
30. L. A. Rahn; R. E. Palmer, J. Opt. Soc. Am. B-Opt. Phys. 3 (9) (1986) 1164-1169
31. A. Bohlin; P. E. Bengtsson; M. Marrocco, J. Raman Spectrosc. 42 (10) (2011) 1843-1847 10.1002/jrs.2869.

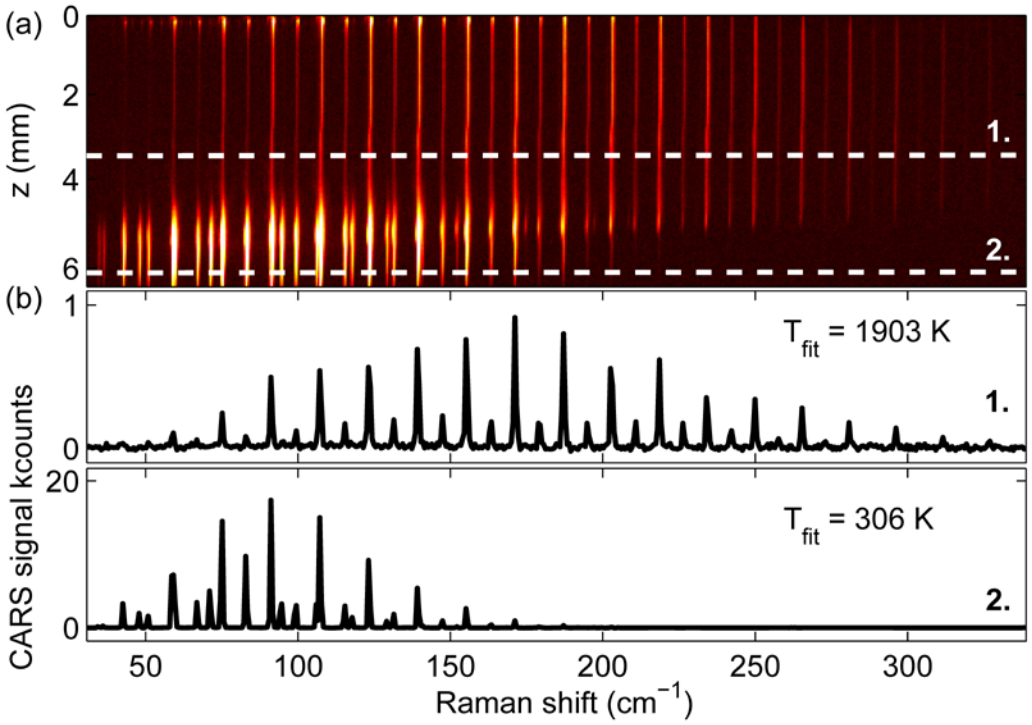

Fig.1. (a) CCD image of the 1D rotational CARS signal obtained from 100 averaged laser shots in the lean Φ=0.8 wall-stabilized flame. The vertical axis is the distance (*z*) from the wall. (b) Two sample row spectra at different distances from the wall with corresponding extracted temperatures.

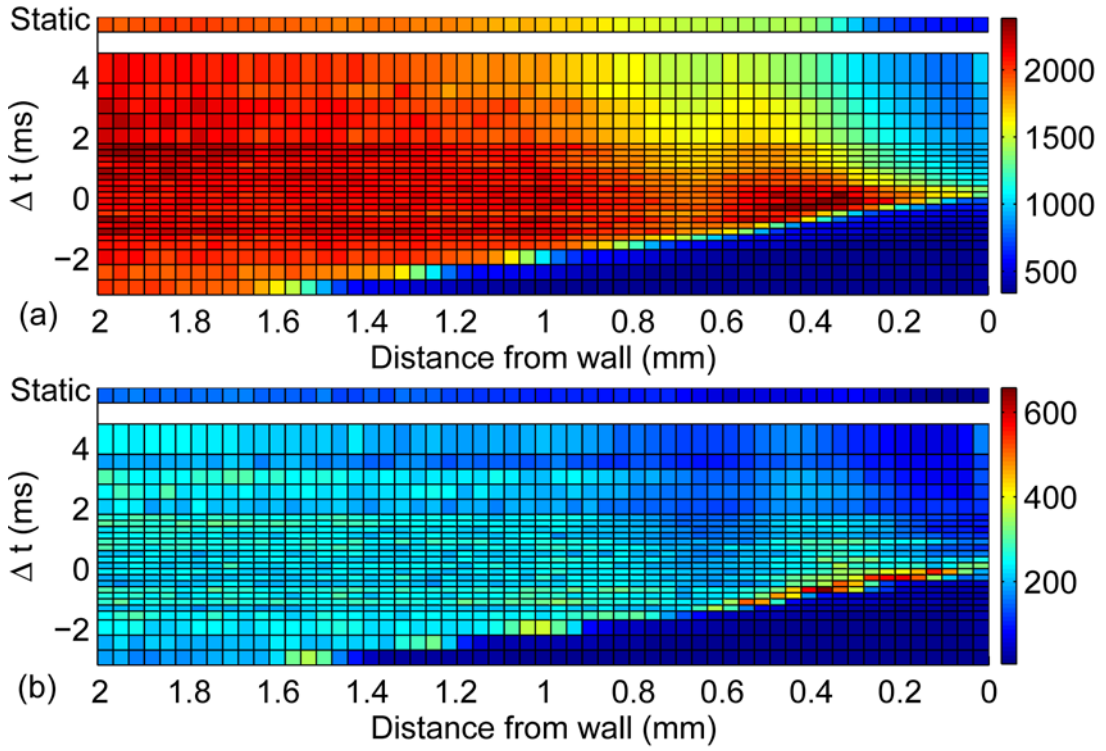

Fig. 2. (a) Evaluated 1D mean temperature profiles as a function of ignition delay time. Equivalence ratio Φ=1.0. Each profile is averaged from 100 single shots. (b) Standard deviation of the evaluated temperatures.

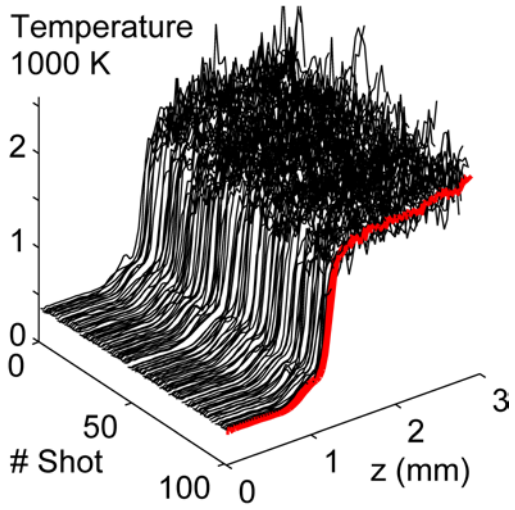

Fig. 3. Evaluated temperature profiles from 100 1D-CARS single shots taken at an ignition delay time (Δt=-2.7 ms) prior to flame interaction with the wall. Φ=1.0.

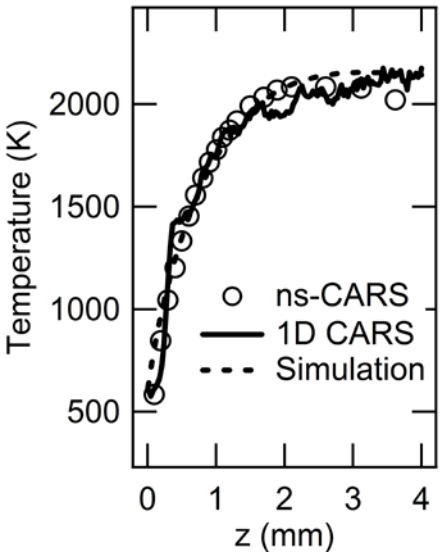

Fig. 4. Comparison of time averaged nanosecond (ns) CARS, two-beam femtosecond/picosecond 1D rotational CARS, and numerical simulation [24] of a wall-stabilized methane/air flame, Φ=1.0.

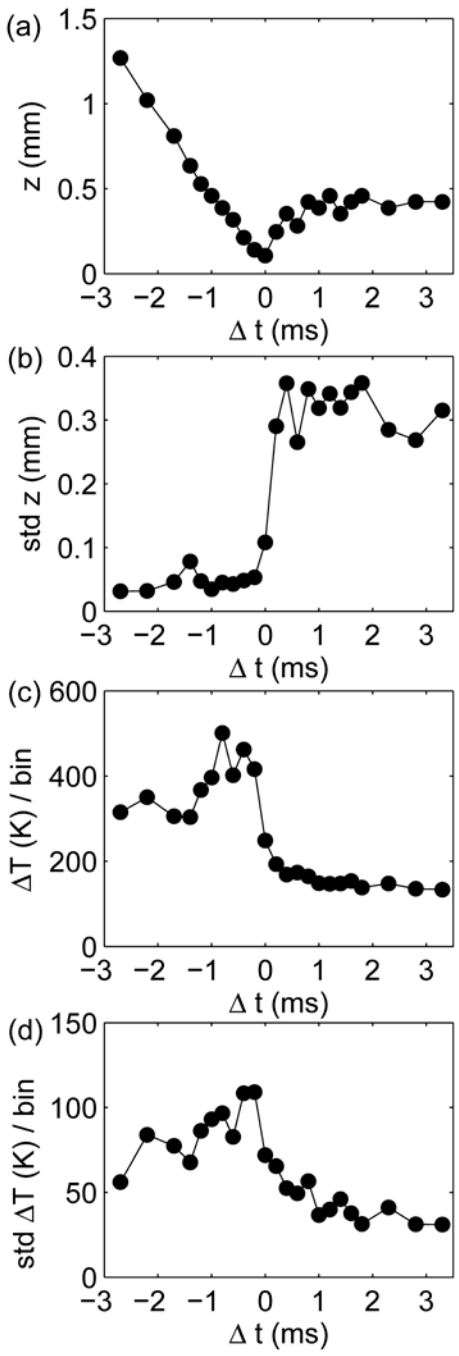

Fig. 5. Evaluated data from single-shot 1D-CARS measurements of HOQ as a function of ignition delay, Δt. Φ=1.0. (a) Flame position. The vertical axis is the distance (*z*) to the wall in mm. (b) Standard deviation of flame position. (c) Maximum flame front temperature gradient as a function of ignition delay. (d) Standard deviation of the maximum flame front temperature gradient.

Figure Captions

Figure 1. (a) CCD image of the 1D rotational CARS signal obtained from 100 averaged laser shots in the lean Φ=0.8 wall-stabilized flame. The vertical axis is the distance (*z*) from the wall. (b) Two sample row spectra at different distances from the wall with corresponding extracted temperatures.

Figure 2. (a) Evaluated 1D mean temperature profiles as a function of ignition delay time. Equivalence ratio Φ=1.0. Each profile is averaged from 100 single shots. (b) Standard deviation of the evaluated temperatures.

Figure 3. Evaluated temperature profiles from 100 1D-CARS single shots taken at an ignition delay time (Δt=-2.7 ms) prior to flame interaction with the wall. Φ=1.0.

Figure 4. Comparison of time averaged nanosecond (ns) CARS, two-beam femtosecond/picosecond 1D rotational CARS, and numerical simulation [24] of a wall-stabilized methane/air flame, Φ=1.0.

Figure 5. Evaluated data from single-shot 1D-CARS measurements of HOQ as a function of ignition delay, Δt. Φ=1.0. (a) Flame position. The vertical axis is the distance (*z*) to the wall in mm. (b) Standard deviation of flame position. (c) Maximum flame front temperature gradient as a function of ignition delay. (d) Standard deviation of the maximum flame front temperature gradient.